

Enhancement of Cooper pair splitting by multiple scattering

Martina Flöser, Denis Feinberg, and Régis Mélin*

Institut NEEL, CNRS and Université Joseph Fourier, BP 166, F-38042 Grenoble Cedex 9, France

In three-terminal NSN hybrid structures the influence of additional barriers on the nonlocal conductance and on current cross-correlations is studied within a scattering theory. In metallic systems with additional barriers and phase averaging, which simulate disordered regions, local processes can be enhanced by reflectionless tunneling but this mechanism has little influence on nonlocal processes and on current cross-correlations. Therefore Cooper pair splitting cannot be enhanced by reflectionless tunneling. On the contrary, in ballistic systems, additional barriers lead to Fabry-Perot resonances and allow to separate the different contributions to the conductance and to the current cross-correlations. In particular, crossed Andreev processes can be selectively enhanced by tuning the length or the chemical potential of the interbarrier region.

PACS numbers: 74.78.Na, 74.45.+c, 72.70.+m

I. INTRODUCTION

Transport in normal metal-superconductor-normal metal (N_aSN_b) hybrid three-terminal nanostructures offers a special interest, owing to the suggestion of producing split pairs of spin-entangled electrons from a superconductor^{1,2}. This is possible when the size of the region separating the N_aS and the N_bS interface becomes comparable to the superconducting coherence length. This circumstance indeed allows coherent processes involving two quasi-particles, each simultaneously crossing one of the two interfaces³⁻⁹. Much effort has been devoted to the theoretical understanding and to the experimental observation of such a Cooper pair splitting effect. In a transport experiment where electrons are difficult to measure one by one — contrarily to the similar production of entangled photons —, one should extract the relevant information from steady transport measurement, e.g. the current-voltage characteristics (conductance) and the cumulants of the current fluctuations (non-equilibrium current noise^{10,11} and its counting statistics¹²). In practice, the conductance and the second-order cumulant (the shot noise and the current cross-correlations between the two current terminals N_a , N_b) are the quantities to be extracted from experiments. Indeed, due to Fermi statistics, the “partition” noise correlations at a three-terminal crossing of normal metal contacts are negative¹⁰, manifesting the antibunching properties of individual electrons. If instead one contact is made superconducting, the cross-correlations may become positive, indicating the splitting of Cooper pairs⁵.

There are two basic nonlocal processes occurring at the double NS interface: Crossed Andreev Reflection (CAR) which alone leads to Cooper pairs splitting into separated electrons bearing opposite spins (for a spin singlet superconductor), and Elastic Cotunneling (EC) which alone leads to (spin-conserving) quasi-particle transmission between the normal contacts, across the superconducting gap⁷. For tunnel contacts, at lowest order in the barrier transparencies, those two processes are simply related to the conductance, leading to positive (resp. nega-

tive) conductance and current cross-correlations for CAR (resp. EC) processes. Indeed Bignon *et al.*¹¹ showed that for tunnel contacts the linear dependence of the current cross-correlation on the voltages applied to the contacts N_a , N_b allows to separately track the amplitudes of CAR and EC. Due to the expected compensation of the opposite CAR and EC conductance components at low transparencies, ferromagnetic contacts are required to detect CAR and EC from the conductance with tunnel contacts^{6,7,13}. Yet, such polarizations are not easily achievable, moreover, if one is interested in producing spin-entangled electrons in a nonlocal singlet state, one should of course not spin polarize the contacts.

Yet, as regards experiments, the situation for (extended) tunnel barriers looks more complicated than given by a simple tunnel model¹⁴. In addition, zero-frequency noise measurements involve weak signals and therefore they require more transparent interfaces, so that the arguments based on a tunnel model cannot be directly applied. For more transparent contacts, it has been found theoretically^{9,15-18} that the nonlocal conductance is dominated by EC thus is negative, which leaves the current cross-correlations as the only possible proof of Cooper pair splitting processes, provided one controls the voltages on both contacts. Contrarily to conductance measurements¹⁹, cross-correlations have led to few experimental results^{20,21}. At the theoretical level, the dependence of the cross-correlations on the contact transparency is not yet fully understood. Further analysis is required if one wishes to extract information from the sign and the amplitude of both the nonlocal conductance and the current cross-correlations in a system where the contacts are non-ferromagnetic metals and the interface transparencies are rather large.

In view of the current experiments on metallic structures, the main question is therefore: Can the cross-correlations be positive, and if the answer is yes, is this a signature of Cooper pair splitting? Previous work on a NSN structure²² showed that the cross-correlations can indeed be positive at large transparencies, although the nonlocal conductance is negative. The origin of this somewhat surprising result was not fully elucidated. Fur-

ther work¹⁸ showed that the sign of the cross-correlations indeed changes with the transparency of the interfaces, being positive at low transparency, negative at intermediate transparency and positive again at high transparency. While the positive sign at low transparency is clearly ascribed to Cooper pair splitting, it was shown that the positive sign at high transparency should not be interpreted in the same way. Indeed, at high transparency, CAR processes do not dominate either in the conductance or in the noise. Instead, the positive cross-correlations should be ascribed to higher order processes, in particular those involving local Andreev reflection (AR) on one side, and the opposite process on the other side, a process equivalent to exchanging a pair of electrons between the two normal contacts.

These results show that transparent interfaces are detrimental to Cooper pair splitting. A possible alternative strategy to boost Cooper pair splitting is to take advantage of multiple scattering to enhance the CAR process. Indeed, at a single NS interface, it was shown that disorder in the N region, or multiple scattering at a clean NN_lS double interface, can strongly enhance Andreev reflection, a mechanism nicknamed "reflectionless tunneling"^{23–25}. With a disordered N' region, it holds below the Thouless energy, where the mutual dephasing of electrons and Andreev-reflected holes is negligible. In the case of a clean double NN_lS interface, maximum Andreev transmission is obtained by balancing the transparencies T_{nn} and T_{ns} of the NN_l and N_lS interfaces, such that the N_l region acts as a resonant cavity. Melsen and Beenakker²⁵ performed an average on the modes inside N_l in order to mimic a disordered region. One can wonder whether a similar mechanism could enhance non-local Andreev reflection e.g. boost CAR compared to AR and EC. For this purpose we consider in this work a set-up $N_aN_lSN_rN_b$ with a quadruple interface. This system can be either considered as a modelization of a true one-dimensional hybrid structure with clean (ballistic) normal and superconducting elements separated by tunnel barriers, for instance using carbon nanotubes or semiconducting nanowires. Or it can mimic a NSN system where the N metals are disordered close to the S interface. A scattering theory is performed in a one-dimensional geometry, varying the transparencies of the barriers and the width of the superconductor.

One important result of this work is the following : If averaging independently the modes in the left and the right regions N_l , no boosting of the CAR process is obtained. Indeed, "reflectionless tunneling" is a quantum coherent process which demands that the Andreev-reflected hole retrace the path of the electron, by scattering on the same impurities. On the contrary, with nonlocal Andreev reflection, the electron and the transmitted hole sample different disorders and no coherence is obtained. Thus, the common reflectionless tunneling mechanism cannot enhance Cooper pair splitting in such a disordered one-dimensional geometry. Interestingly, we show that if on the contrary the N_l regions can be tuned

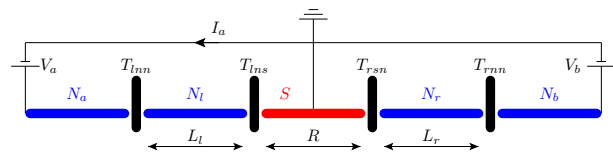


Figure 1: Schematic of the model.

at a Fabry-Perot resonance for the specific electron and Andreev-transmitted hole wavevectors, then CAR can be efficiently enhanced, moreover CAR and EC processes can be filtered at will by tuning the energy or the Fermi wavevector of both N_l region. The feasibility of such a proposal is discussed at the end.

Section II presents the model and section III the scattering theory of the $N_aN_lSN_rN_b$ system. Section IV provides the results obtained by averaging over channels in N_l and N_r , in the spirit of Ref. 25. Section V describes transport in the case where N_l and N_r are clean metallic "cavities". Section VI concludes by discussing a possible implementation of a controllable Cooper pair splitter.

II. THE MODEL

We study a one-dimensional model of a symmetrical three-terminal normal metal-superconductor-normal metal hybrid structure depicted in Fig. 1. The central superconducting electrode is grounded, the normal terminals can be biased with voltages V_a and V_b . The length R of the superconducting electrode is comparable to the superconducting coherence length, which makes the observation of nonlocal effects possible. The interfaces between the normal metal and the superconducting electrodes are modeled by barriers with transparencies T_{lns} and T_{rsn} . In both normal metal electrodes there is an additional barrier at a distance L_l (respectively L_r) from the normal metal superconductor interface with transparency T_{lnn} (respectively T_{rnn}).

The system can be described by a 4×4 scattering matrix $s_{ij}^{\alpha\beta}$ where Latin indices run over the normal electrodes a and b and Greek indices over electrons e and holes h . For energies lower than the superconducting gap, there are no single electron or hole states in the bulk of the superconducting electrode. Consequently, there is no scattering of electrons or holes in or out of the reservoir in the superconducting electrode and the latter does not appear in the scattering matrix. However, the scattering theory implicitly assumes that the superconductor is a reservoir of Cooper pairs. It is thus essential that the superconducting electrode is grounded. The transformation of quasi-particles into Cooper pairs is taken into account by the correlation length ξ which sets the scale of the damping of the electron and hole wavefunctions in the superconductor.

The elements of the scattering matrix are evaluated from the BTK approach²⁶ (see Appendix A). As the energy dependence of the calculated quantities is relevant, we do not use the Andreev approximation valid in the limit of zero energy where the electron and hole wavevectors are set to the Fermi wavelength, but instead keep the full expressions for the wave vectors. The calculation of the average current and current cross-correlations rely on the formulas obtained by Anantram and Datta in Ref. 27:

$$I_i = \frac{e}{h} \sum_{k \in \{a,b\}} \sum_{\alpha, \beta \in \{e,h\}} \text{sgn}(\alpha) \quad (1)$$

$$\times \int dE \left[\delta_{ik} \delta_{\alpha\beta} - |s_{ik}^{\alpha\beta}|^2 \right] f_{k\beta}(E)$$

$$S_{ij} = \frac{2e^2}{h} \sum_{k,l \in \{a,b\}} \sum_{\alpha, \beta, \gamma, \delta \in \{e,h\}} \text{sgn}(\alpha) \text{sgn}(\beta) \quad (2)$$

$$\times \int dE A_{k\gamma, l\delta}(i\alpha, E) A_{l\delta, k\gamma}(i\alpha, E) f_{k\gamma}(E) [1 - f_{l\delta}(E)]$$

with $A_{k\gamma, l\delta}(i\alpha, E) = \delta_{ik} \delta_{il} \delta_{\alpha\gamma} \delta_{\alpha\delta} - s_{ik}^{\alpha\gamma\dagger} s_{il}^{\alpha\delta}$, $\text{sgn}(\alpha = e) = 1$, $\text{sgn}(\alpha = h) = -1$, $f_{i\alpha}$ the occupancy factors for the electron and hole states in electrode i , given by the Fermi function where the chemical potential are the applied voltages $f_{ie}(E) = \left[1 + \exp\left(\frac{E - V_i}{k_B T}\right) \right]^{-1} \xrightarrow{T \rightarrow 0} \theta(-E + V_i)$, $f_{ih}(E) = \left[1 + \exp\left(\frac{E + V_i}{k_B T}\right) \right]^{-1} \xrightarrow{T \rightarrow 0} \theta(-E - V_i)$.

In this one-dimensional model, both current and noise are highly sensitive to the distances L_l, R, L_r between the barriers: They oscillate as a function of these distances with a period equal to the Fermi wavelength $\lambda_F \ll L_l, R, L_r$. In a ballistic system, the multiple barriers act like a Fabry-Perot interferometer and the interference ef-

fects are studied in section V. In a higher-dimensional system with more than one transmission mode, the oscillations in the different modes are independent and are thus averaged out. Multidimensional behavior can be simulated qualitatively with a one-dimensional system by averaging all quantities over one oscillation period:

$$\begin{aligned} \overline{X}(L_l, R, L_r) & \quad (3) \\ &= \frac{1}{\lambda_F^3} \int_{L_l - \frac{\lambda_F}{2}}^{L_l + \frac{\lambda_F}{2}} dl_l \int_{R - \frac{\lambda_F}{2}}^{R + \frac{\lambda_F}{2}} dr \int_{L_r - \frac{\lambda_F}{2}}^{L_r + \frac{\lambda_F}{2}} dr X(l_l, r, l_r). \end{aligned}$$

This procedure is appropriate to describe metallic systems. These averaged quantities are studied in section IV.

III. COMPONENTS OF THE DIFFERENTIAL CONDUCTANCE AND THE DIFFERENTIAL CURRENT CROSS-CORRELATIONS

An electron, arriving from one of the normal metal reservoirs at the interface to the superconductor, can have four different destinies: It can be reflected as an electron (normal reflection (NR)), or reflected as a hole (Andreev reflection (AR)), or transmitted as an electron (elastic cotunneling (EC)) or transmitted as a hole (crossed Andreev reflection (CAR)), and similarly for holes. The corresponding elements of the scattering matrix are for NR: $s_{aa}^{ee}, s_{aa}^{hh}, s_{bb}^{ee}, s_{bb}^{hh}$, AR: $s_{aa}^{eh}, s_{aa}^{he}, s_{bb}^{eh}, s_{bb}^{he}$, EC: $s_{ab}^{ee}, s_{ab}^{hh}, s_{ba}^{ee}, s_{ba}^{hh}$, and CAR: $s_{ab}^{eh}, s_{ab}^{he}, s_{ba}^{eh}, s_{ba}^{he}$.

The current in electrode N_a given by Eq. (1) can naturally be divided into AR, CAR and EC contributions (to calculate this expression the unitarity of the scattering matrix has been used):

$$\begin{aligned} I_a = \frac{|e|}{h} \int dE & \underbrace{[|s_{aa}^{eh}(E)|^2 + |s_{aa}^{he}(E)|^2]}_{\text{local Andreev reflection}} (f_{ae}(E) - f_{ah}(E)) \\ & + \underbrace{[|s_{ab}^{ee}(E)|^2 (f_{ae}(E) - f_{be}(E)) + |s_{ab}^{hh}(E)|^2 (f_{bh}(E) - f_{ah}(E))]}_{\text{elastic cotunneling}} \\ & + \underbrace{[|s_{ab}^{eh}(E)|^2 (f_{ae}(E) - f_{bh}(E)) + |s_{ab}^{he}(E)|^2 (f_{be}(E) - f_{ah}(E))]}_{\text{crossed Andreev reflection}}. \quad (4) \end{aligned}$$

In the following, we focus on i) the differential conductance in the symmetrical case where $V_a = V_b = V$ and the current I_a is differentiated with respect to V , and ii) the differential nonlocal conductance in the asymmetrical case where $V_a = 0$ and the current I_a is differentiated with respect to V_b . In the zero temperature limit, only the nonlocal processes, CAR and EC, contribute to the nonlocal conductance:

$$\left. \frac{\partial I_a}{\partial V_b} \right|_{V_a=0} = \underbrace{-\frac{e^2}{h} [|s_{ab}^{ee}(|e|V_b)|^2 + |s_{ab}^{hh}(-|e|V_b)|^2]}_{\text{elastic cotunneling}} + \underbrace{\frac{e^2}{h} [|s_{ab}^{eh}(-|e|V_b)|^2 + |s_{ab}^{he}(|e|V_b)|^2]}_{\text{crossed Andreev reflection}}, \quad (5)$$

while the symmetric case contains local Andreev reflection and crossed Andreev reflection:

$$\begin{aligned} \left. \frac{\partial I_a}{\partial V} \right|_{V_a=V_b=V} &= \frac{e^2}{h} \underbrace{[(|s_{aa}^{eh}(|e|V)|^2 + |s_{aa}^{he}(|e|V)|^2) + (|s_{aa}^{eh}(-|e|V)|^2 + |s_{aa}^{he}(-|e|V)|^2)]}_{\text{local Andreev reflection}} \\ &+ \frac{e^2}{h} \underbrace{[(|s_{ab}^{eh}(|e|V)|^2 + |s_{ab}^{he}(|e|V)|^2) + (|s_{ab}^{eh}(-|e|V)|^2 + |s_{ab}^{he}(-|e|V)|^2)]}_{\text{crossed Andreev reflection}} \end{aligned} \quad (6)$$

Let us now perform a similar analysis for the current cross-correlations. We study only the zero temperature limit, where $f_{k\gamma}(E)[1 - f_{l\delta}(E)]$ is zero if $k = l$ and $\gamma = \delta$ and the current cross-correlations are:

$$S_{ab}(T = 0) = \frac{2e^2}{h} \sum_{k,l \in \{a,b\}} \sum_{\alpha,\beta,\gamma,\delta \in \{e,h\}} \text{sgn}(\alpha)\text{sgn}(\beta) \int dE s_{ak}^{\alpha\gamma\dagger} s_{al}^{\alpha\delta} s_{bl}^{\beta\delta\dagger} s_{bk}^{\beta\gamma} f_{k\gamma}(E)[1 - f_{l\delta}(E)] \quad (7)$$

Every summand in S_{ab} contains the product of four elements of the scattering matrix. As pointed out in Refs. 28,29, in difference to the situation for the current, it is impossible to combine those matrix elements to absolute squares. Let us now try to classify the contributions of the noise as we did above for the current. We find that no summand consists of only one kind of elements of the scattering matrix. Every element consists of two local elements (NR or AR) and two nonlocal elements (CAR or EC). Either the two local elements and the two nonlocal elements are identical, that gives the components EC-NR, CAR-NR, EC-AR, CAR-AR, or all four matrix elements belong to different categories and we will call these summands MIXED. Sometimes, it is useful to divide MIXED further as a function of its voltage dependence (see Appendix B). As the formulas for the current cross correlations are lengthy, they are relegated into appendix B.

For the interpretation of current cross-correlations, the global sign plays an important role. For positive applied bias voltages, the differential current cross-correlations carry the same sign as the current cross-correlations. For negative applied voltages current, cross-correlations and differential current cross-correlations have opposite signs. To avoid confusion, we only show pictures of the differential current cross-correlations calculated for positive bias voltages (and thus negative energies $E = -|e|V$). Due to the electron-hole symmetry of the model, differential current cross-correlations calculated for negative bias voltages are up to a global sign identical to the ones calculated at positive bias voltage. For small bias voltages, current cross-correlations depend linearly on voltage. Thus, current cross-correlations and differential current cross-correlations show the same qualitative behavior if studied as a function of the interface transparency or the distance between barriers.

In Ref. 18, we performed a similar analysis of current cross-correlations in terms of Green's functions. For the relations between these two classifications see Appendix C.

Bignon *et al.*¹¹ have studied current cross-correlations in the tunneling limit. They find that noise measurements in the tunneling limit can give access to the CAR and EC contribution of the current. We have just seen, that at least two processes are involved in every component of noise, but the contributions of noise they calculate fall into the categories EC-NR and CAR-NR. In the tunneling limit the NR contribution is so close to one, that it can be neglected and what remains is very similar to the current contributions.

IV. THE AVERAGED SYSTEM

A. Positive Cross-Correlations without CAR

In fermionic systems without superconducting electrodes, current cross-correlations are, as a consequence of the Fermi-Dirac statistics, always negative^{10,27}. In superconductors, on the contrary, the coupling of electrons into Cooper pairs makes positive cross-correlations possible⁵. If a CAR process is interpreted as the splitting of a Cooper pair into two electrons leaving the superconductor in different electrodes, positive cross-correlations are its logical consequence. However, the CAR process is not the only one which can lead to positive cross-correlations. Let us investigate in more detail the influence of the different processes on the current cross-correlations in a NSN-system, i.e. in a system without the additional barriers in the normal conducting electrodes.

The black line in Figure 2 shows the averaged differential current cross-correlations for symmetric bias ($V = V_a = V_b$). The total current cross-correlations have already been published in Ref. 18, but here, Figure 2 shows in addition the different parts which contribute to the total current cross-correlations. The total cross-correlations are positive for high interface transparencies and for low interface transparencies. As we have already argued in Ref. 18, the positive cross-correlations at high

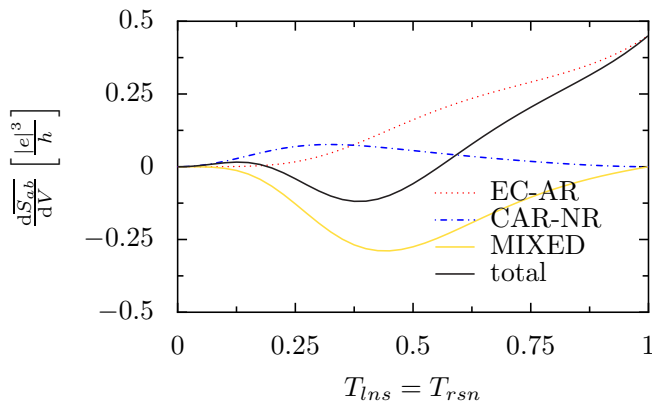


Figure 2: Averaged differential current cross-correlations for a symmetrical biased ($V = V_a = V_b \ll \Delta/|e|$) NSN-system as a function of the transparency of the interfaces $T_{lns} = T_{rsn}$. The positive cross-correlations at high interface transparency are due to the EC-AR process, represented by a dotted line.

interface transparencies are not due to CAR. Indeed, at very high transparencies, only processes which conserve momentum can occur, since there are no barriers which can absorb momentum. CAR processes do not conserve momentum: if e.g. an electron arrives from the left hand side carrying momentum k_F , the hole that leaves at the right hand side carries momentum $-k_F$. As the cross-correlations do not tend to zero even for very high transparencies, they cannot be due to CAR. Indeed, if we plot the different components of the noise introduced in the last section separately, we see that positive current cross-correlations at low interface transparencies are a consequence of a large CAR-NR component and therefore a consequence of CAR processes. But the positive current cross-correlations at high interface transparencies have a different origin: a large positive EC-AR contribution.

We can put the contributions to the current cross-correlations into two categories with respect to their sign, which is independent of the interface transparency. EC-NR, CAR-AR, MIXED2 and MIXED4 carry a negative sign, CAR-NR, EC-AR, MIXED1 and MIXED3 carry a positive sign. The current can either be carried by electrons I^e or by holes I^h . The sign of the different contributions to the current cross-correlations depends on whether only currents of the same carrier type are correlated²⁷ ($\langle \Delta \hat{I}_a^e \Delta \hat{I}_b^e \rangle + \langle \Delta \hat{I}_a^h \Delta \hat{I}_b^h \rangle + a \leftrightarrow b$), which is the case for EC-NR, CAR-AR, MIXED2 and MIXED4 and leads to a negative sign; or whether electron currents are correlated with hole currents ($\langle \Delta \hat{I}_a^e \Delta \hat{I}_b^h \rangle + \langle \Delta \hat{I}_a^h \Delta \hat{I}_b^e \rangle + a \leftrightarrow b$), which is the case for CAR-NR, EC-AR, MIXED1 and MIXED3 and leads to a positive sign. In purely normal conducting systems, the electron and hole currents are uncorrelated, only correlations of the same carrier type contribute to the current cross-correlation and lead to a negative sign. The sign of the total current cross-correlations is a consequence of the relative strength of the different parts of the current cross-correlations, which depends on the interface transparency.

B. Multiple Barriers

In the last paragraph, we learnt that positive cross-correlations due to CAR can only be found in the tunneling regime. But in the tunnel regime the signals are quite weak. The conductance over an NS-tunnel junction can be larger for a “dirty” normal conductor containing a large number of non-magnetic impurities, where transport is diffusive, than for a clean normal conductor, where transport is more ballistic, by an effect called reflectionless tunneling^{23,24}. It is thus natural to ask if a similar effect could also enhance conductance and current cross-correlations in a three terminal NSN-structure. To answer this question, we use the model of Melsen and Beenakker²⁵ where the disordered normal conductor is replaced by a normal conductor with an additional tunnel barrier leading to an NNS structure. Duhot and Mélin¹⁵ have studied the influence of additional barriers on the nonlocal conductance in three terminal NSN-structures. They find that two symmetric additional barriers enhance the nonlocal conductance.

First, let us get a deeper understanding of their result by calculating the AR, CAR and EC components of the current separately. Afterwards, we will study the influence of additional barriers on the current cross-correlations.

Figure 3 shows the averaged conductivity in the symmetrical bias situation $V_a = V_b \ll \Delta/|e|$ and in the asymmetrical voltage case $V_a = 0, V_b \ll \Delta/|e|$ for a superconducting electrode much shorter than the coherence length ($R = 0.25\xi$). The sum of the AR, CAR and EC components, traced in black, features in both cases an extremum. Yet, looking at the behavior of these components, we see that they arise from different mechanisms. Let us first have a look at the symmetrically biased case. Without the additional barriers, i.e. in the limit $T_{lnn} = T_{rnn} \rightarrow 1$, the contributions of AR and CAR are similar in magnitude. The EC component is completely suppressed, since it is proportional to the difference of the applied voltages. The introduction of two additional barriers increases the AR component by about a factor 30. The shape of the curves is similar to the one of the NNS structure derived analytically by Melsen and Beenakker²⁵, which can be recovered exactly by increasing the length of the superconducting electrode far beyond the coherence length. However, the CAR curve stays almost constant over a wide range of values of barrier strength of the additional barriers, and it eventually vanishes when the transparencies go to zero.

In the asymmetrical voltage case $V_a = 0$, the AR component is zero as it is proportional to the local voltage V_a . Like in the first case, the additional barriers have little influence on the CAR component, except for the fact that it tends to zero for vanishing transparency. Over a wide range of barrier strength values, the EC component is identical in amplitude, but opposite in sign to the CAR component. For small $T_{lnn} = T_{rnn}$ values the EC component displays a small extremum, but it is much

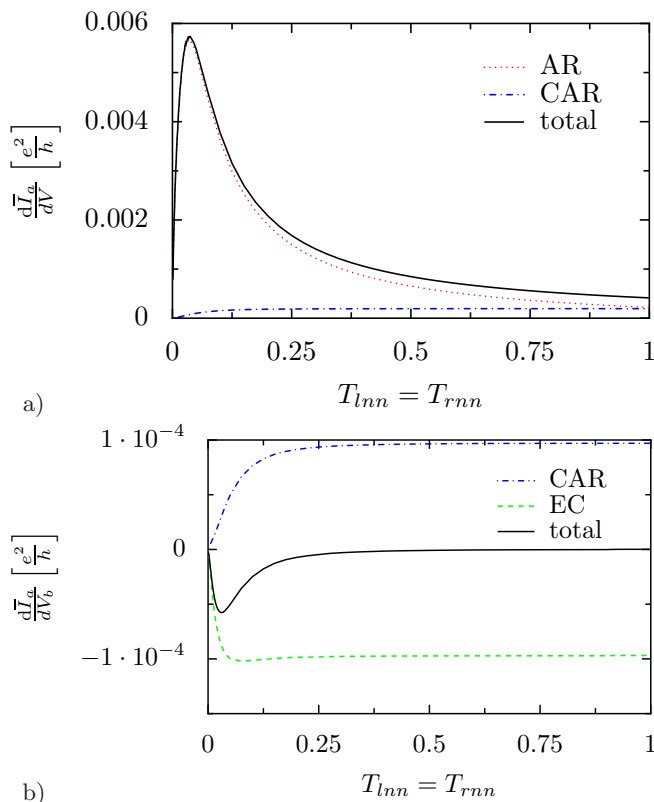


Figure 3: Averaged differential conductance in the limit of zero energy in a) the symmetrical bias situation $V_a = V_b \ll \Delta/|e|$ and b) in the asymmetrical case $V_a = 0, V_b \ll \Delta/|e|$ for a superconducting electrode much shorter than the coherence length ($R = 0.25\xi$) as a function of the transparencies of the additional barriers $T_{lnn} = T_{rnn}$. The barriers next to the superconductor are in the tunnel regime ($T_{lns} = T_{rsn} = 0.01$).

less pronounced than the maximum of the AR component of the first case. In the limit $T_{lnn} = T_{rnn} \rightarrow 1$, the EC component tends more slowly to zero than the CAR component which as a consequence has a minimum in the total conductance. The fact that the conductance maxima in the symmetrical bias case and in the asymmetrical bias case have different origins can also be illustrated by studying their energy dependence, depicted in Figure 4: The enhancement of the AR component of the conductance in the symmetrical biased case disappears completely with increasing bias voltage. The extremum of the conductance in the asymmetrical biased case decreases slightly with increasing bias voltage, but only up to a certain voltage value, then it saturates.

Why is the AR component enhanced by the additional barriers, but not the EC or CAR components? Reflectionless tunneling is believed to occur because the electrons and holes get localized between the double barrier and have therefore a higher probability to enter the superconductor. There is a double barrier on the right and on the left hand side, so this localization should also happen to the particles involved in EC or CAR processes. The answer is, that in the AR cases the incoming elec-

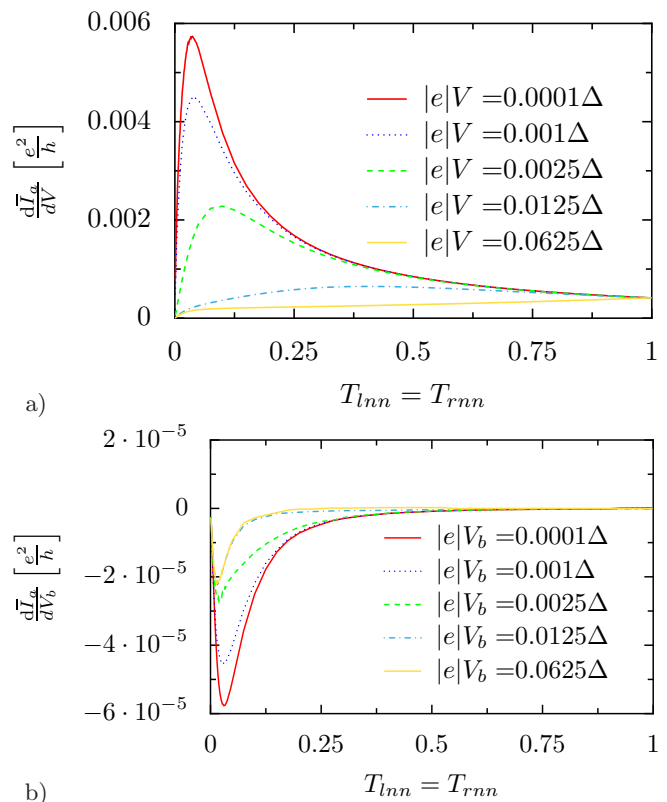


Figure 4: Total averaged differential conductance, as in Figure 3 but at different energies.

tron and the leaving hole see the same environment. In the EC and CAR process, the incoming particle sees the environment on one side of the superconductor and the leaving particle the environment on the other side. The energy dependence of the conductance enhancement of the AR component demonstrates that reflectionless tunneling can only occur if the outgoing hole can trace back the way of the incoming electron. At low bias voltages where the electron and the hole have nearly the same energy and wavevector, reflectionless tunneling occurs. At higher bias voltage, electrons and holes have different wavevectors and the reflectionless tunneling peak disappears. The integrals over the phases between the additional barriers on the left- and on the right-hand side have, of course, been taken independently. There is no reason to think that the channel mixing, which is emulated by the integrals, on the left- and on the right-hand side are coupled. To verify this scenario, let us couple the two integrals in an gedankenexperiment. We set the distance L_l between the two left-hand side barriers to be equal to the distance L_r between the two right-hand side barriers and perform only one integral over $L = L_l = L_r$. The result is shown in Figure 5. Now, the CAR and the EC component are also enhanced. Still, the effect on the EC component is larger and EC dominates the nonlocal conductance.

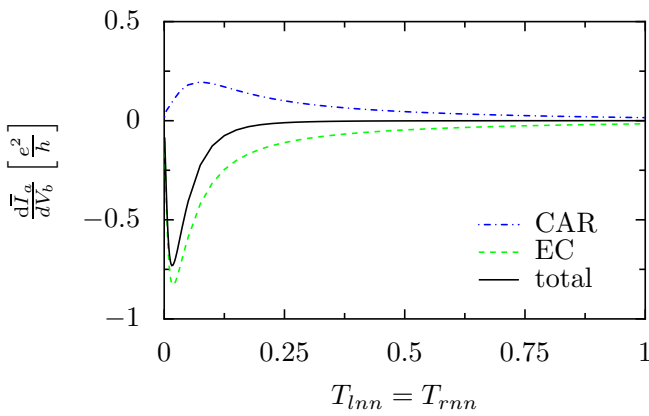


Figure 5: Gedankenexperiment with coupled integrals $T_{lns} = T_{rsn} = 0.01$, $R = 0.25\xi$: Now, also the EC and the CAR component are enhanced by reflectionless tunneling.

Let us turn back to independent averaging and have a look at the current cross-correlations shown in figure 6. In the symmetrical bias case, the additional barriers do not lead to an enhancement of the signal. The noise is dominated by the CAR-NR component, and, as we have seen above, CAR is not influenced by reflectionless tunneling. The EC-AR component is amplified by the additional barriers, because the AR amplitude describing a local process is amplified. This leads to a small shoulder in the total cross-correlations. But since we are in the tunnel regime and the leading order of CAR-NR is T^2 while the leading order of EC-AR is T^4 , the influence of the EC-AR-component is too small to lead to a global maximum.

In the asymmetrical bias case $V_a = 0, V_b \ll \Delta/|e|$, on the other hand, the additional barriers enhance the signal. But the cross-correlations are dominated by EC-NR and are therefore negative. We conclude that in a phase-averaged system, additional barriers only enhance the AR-component, a local process. It cannot help to amplify nonlocal signals. Thus, positive cross-correlations, when due to nonlocal processes cannot be enhanced with additional barriers if an average over the length has to be done.

V. THE BALLISTIC SYSTEM

In a last step, let us examine if the additional barriers can enhance the current cross-correlations in a ballistic one-channel device, where no integrals over the length of the normal conducting channels need to be done. We nevertheless maintain the average over the central superconducting electrode. One can indeed imagine that the normal conducting channels are formed by single-wall nano-tubes, where transport is ballistic, while the superconducting central electrode is made from more disordered aluminum.

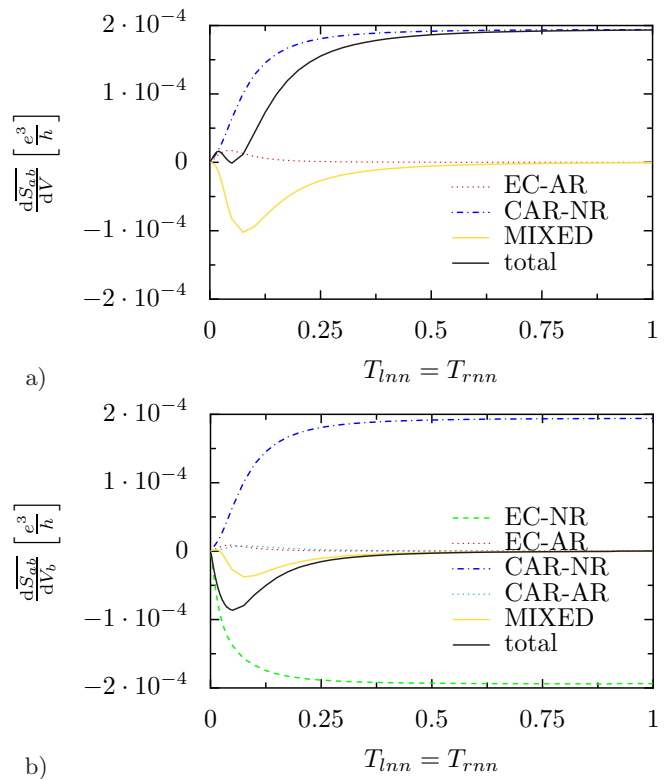


Figure 6: Averaged differential current cross-correlations in a) the symmetrical bias situation $V_a = V_b \ll \Delta/|e|$ and b) the asymmetrical bias case $V_a = 0, V_b \ll \Delta/|e|$ for a superconducting electrode shorter than the coherence length ($R = 0.25\xi$) as a function of the transparencies of the additional barriers $T_{lnn} = T_{rnn}$. The barriers next to the superconductor are in the tunnel regime ($T_{lns} = T_{rsn} = 0.01$).

A. Resonances in a Fabry-Perot Interferometer

Assuming ballistic transport in the normal conducting parts, the NNSNN-system consists in principle of two Fabry-Perot interferometers, one at the left- and one at the right-hand side of the superconductor. For the final result the entire system has to be taken into account. But thinking of the two Fabry-Perot interferometers independently already gives a fair idea of where to expect resonance peaks, and what influence they have on the different components of the conductance and of the current cross-correlations.

In an optical Fabry-Perot interferometer consisting of two parallel mirrors, the transmitted intensity results from the interference of light which has undergone multiple reflections between the two mirrors. The transmission of a Fabry-Perot interferometer is a function of the phase difference between a beam which has been n -times and a beam which has been $(n+1)$ -times reflected at both interfaces. The same is true for a Fabry-Perot interferometer for electrons. An electron going once back and forth between the two barriers at the left-hand side of the NNSNN-system acquires a phase $\phi^e = 2q^+L_l$,

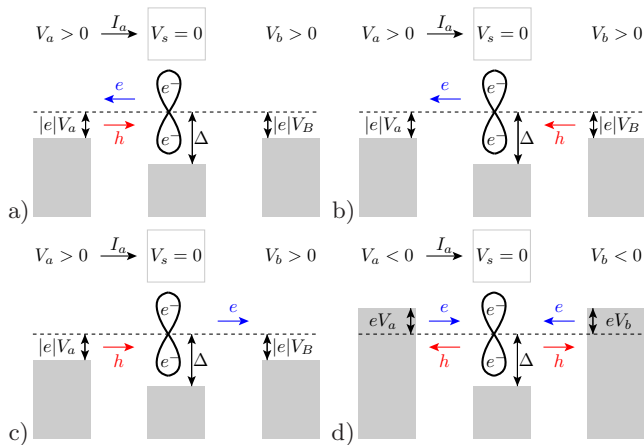


Figure 7: Schematics of the contributions to the conductance in the symmetrically biased case. The filled states are depicted in the three reservoirs, together with the electron and hole currents between the barriers. a) AR contribution for positive bias, b) and c) The two possible CAR contributions for positive bias, d) Summary of the processes for negative bias. If negative voltages are applied, the roles of electrons and holes are interchanged, but the resulting conductance stays unchanged.

a hole acquires a phase $\phi^h = 2q^-L_l$, where q^+ is the wavevector of the electrons and q^- the wavevector of the holes. For low voltages, where $q^+ \approx q^-$, we expect electron and hole resonances to happen for the same resonator lengths. If the voltage is increased, the wavevector $q^+ = \sqrt{2m\hbar^2\sqrt{\mu - |e|V}}$ decreases and the wave vector $q^- = \sqrt{2m\hbar^2\sqrt{\mu + |e|V}}$ increases, shifting the resonance for electrons to higher and the resonance for holes to lower values of L_l . The width of the resonances of a Fabry-Perot interferometer decreases as the reflectivity of the interfaces increases.

1. Symmetrically applied bias

For a symmetrically applied bias, the differential conductance consists of an AR and a CAR component. If a positive bias is applied to the normal electrode N_a , the current I_a contains an AR contribution, where a hole enters and an electron leaves the superconductor (see figure 7a). At low energies, the AR contribution will have a maximum for values of L_l where electrons and holes are both in resonance. At higher energies, the resonances for electrons and for holes occur at different values of L_l . If the barriers are in the tunnel regime, the resonance peaks are sharp. The resonance peaks for electrons and holes stop overlapping and the AR contribution disappears. If the interface transparency is increased, the resonance peaks broaden. Even if the electron and the hole wavevectors are significantly different, there is an overlap between corresponding resonances leading to a double peak in the AR contribution. AR is a local process, and

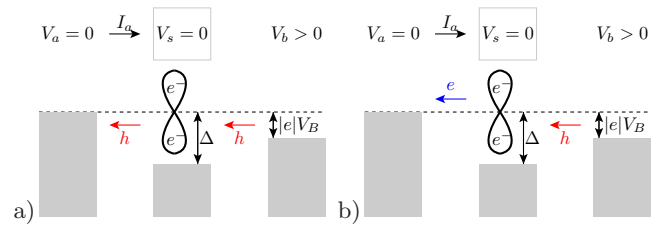


Figure 8: Schematics of the contributions to the conductance in the asymmetrically biased configuration. The filled states are depicted in the three reservoirs, together with the current of electrons and holes between the barriers. a) EC contribution for positive bias, b) CAR contribution for positive bias.

we expect the AR contribution to the current I_a to be mainly independent of the length L_r .

There are two possibilities for CAR process if the electrodes N_a and N_b are symmetrically and positively biased: Either a hole enters the superconductor at the left-hand side and an electron leaves the superconductor at the right-hand side (see figure 7b); or the process occurs the other way around (see figure 7c), the hole enters at the right-hand side and the electron leaves at the left-hand side. In a CAR process, both sides are involved and the position of the resonances will be a function of both L_l and L_r . At low energies, the resonances for the two CAR processes will be superimposed and occur at length values $L_l = L_r \text{ mod } \pi/k_F$. In a CAR process, the incoming hole and the outgoing electron are spatially separated. It is therefore possible to reach the optimal resonance condition for electrons and for holes even if the two kinds of carriers have different wavevectors. For higher bias values, the conductance maximum due to the CAR process sketched in figure 7b will be shifted to lower values of L_l and higher values of L_r . It will be the other way around for the conductance maximum due to the second CAR process. Therefore, we expect the resonance peak to split up into two peaks.

CAR and AR both have a positive contribution to the differential conductance. This can also be seen in figure 7: The current I_a is defined as positive if positive charges enter the superconductor. On the left-hand side, all electrons leave the superconductor and all holes enter it. If a negative bias is applied instead of a positive one, electrons and holes will interchange their roles (see figure 7d). The resonance positions and the sign of the conductance, however, will not change because $q^+(V) = q^-(-V)$.

2. Asymmetrically applied bias $V_a = 0, V_b > 0$

Let us now focus on the bias configuration $V_a = 0, V_b > 0$ used to measure a nonlocal conductance. The latter consists of an EC and a CAR contribution. EC processes involve the same type of charge carriers on both sides of the superconductor. Therefore, the resonances for EC will always occur for diagonal values $L_l = L_r \text{ mod } \pi/k_F$.

At positive bias, EC is carried by holes (see figure 8a) and if the voltage is increased, the resonances in L_l and L_r are simultaneously shifted to lower values. EC leads to a negative differential conductance as the holes move out of the superconductor and the current is defined positive when entering the superconductor.

From the two kinds of possible CAR processes in the symmetrically biased case, only the second one contributes to the nonlocal conductance. At low energies the EC and the CAR peak will be superimposed. At higher energies, the CAR peak moves away from the diagonal. The application of a negative bias again interchanges the roles of electrons and holes, but it does not influence the resonance positions. The only difference between a positive and a negative applied bias is the global sign of the current cross-correlations.

If one wishes to use a Fabry-Perot interferometer as a filter for the different processes contributing to the conductance and to the current cross-correlations, we expect that it will be essential to operate the system at energies where the wavevectors of electrons and holes are significantly different. In the next section, numerical results will be analyzed, which will turn out to be in qualitative agreement with the scenario discussed in this section. We start with the tunnel regime, then investigate how the contrast diminishes with increasing interface transparency and eventually have a closer look at a system with intermediate interface transparencies.

B. The Tunnel Regime

Let us now discuss the calculated conductance and the current cross-correlations. In a first step, the barriers between the superconducting and the normal regions are chosen to be in the tunnel regime ($T_{lns} = T_{rsn} \approx 0.01$) in order to achieve sharp resonances. The distances L_l and L_r are of the order of ten times the coherence length ξ . This distance allows to observe phase differences $\Delta\phi = |\phi^e - \phi^h|$ of the order of 2π between electrons and holes already at energies much smaller than the superconducting gap.

As for the averaged system, we will study four different quantities: the conductance in the symmetrically biased case, the nonlocal conductance, where the normal electrode in which the current is calculated is at the same potential as the superconductor, and the current cross-correlations in the same two bias configurations. The results are presented in the figures 9, 10, 11 and 12. The panels a) and c) always show a three-dimensional plot of the conductance (respectively the current cross-correlations) as a function of the distances between the barriers L_l and L_r . The three-dimensional plot in panel a) always depicts the situation in the limit of zero energy. The one in panel c) refers to higher energies. The three-dimensional plots are completed by cuts through the resonances. These cuts show the different contributions in different colors and have a higher resolution.

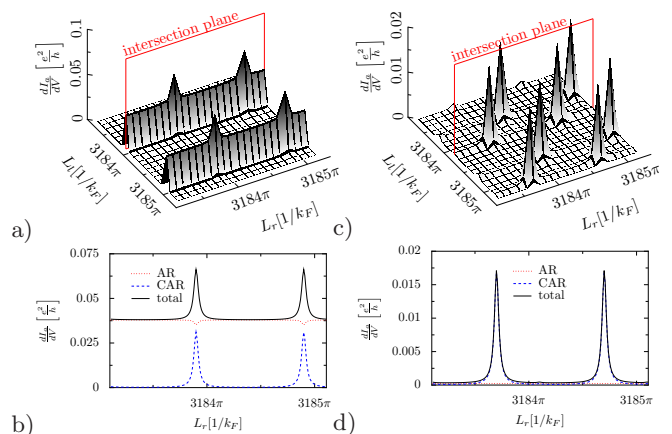


Figure 9: Differential conductance for symmetrically applied bias $V = V_a = V_b$ in the tunneling limit $T_{lns} = T_{rsn} = 0.01$, $T_{lnn} = T_{rnn} = 0.26$, a) as a function of L_r and L_l at low voltage $|e|V = 1 \cdot 10^{-4}\Delta$, b) cut through a) along one of the "mountain ranges" (at $L_l = 3183.9\pi/k_F$) at higher resolution, c) as a function of L_r and L_l at higher voltage $|e|V = 6.25 \cdot 10^{-2}\Delta$, d) cut through c) at $L_l = 3184.1\pi/k_F$ at higher resolution.

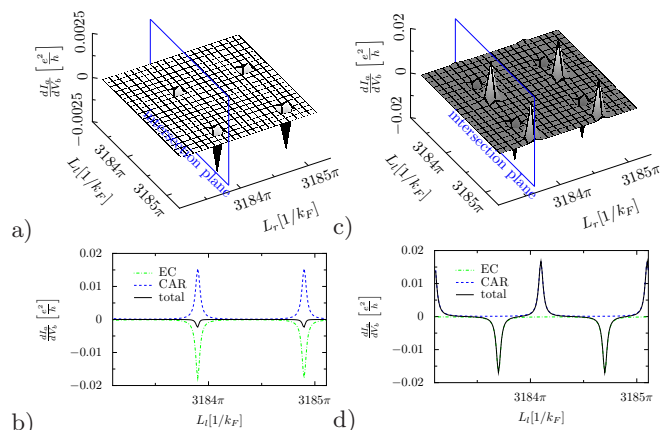


Figure 10: Differential nonlocal conductance ($V_a = 0$) in the tunneling limit $T_{lns} = T_{rsn} = 0.01$, $T_{lnn} = T_{rnn} = 0.26$, a) as a function of L_r and L_l at low voltage $|e|V_b = 1 \cdot 10^{-4}\Delta$, b) cut through a) at $L_r = 3183.9\pi/k_F$ at higher resolution, c) as a function of L_r and L_l at higher voltage $|e|V_b = 6.25 \cdot 10^{-2}\Delta$, d) cut through c) at $L_r = 3183.6\pi/k_F$ at higher resolution.

1. Conductance for a symmetrically biased system

Figure 9a shows the differential conductance $dI_a/dV|_{V=V_a=V_b>0}$ in the symmetrically biased case $V_a = V_b$ as a function of the distances L_l and L_r in the limit $V \rightarrow 0$. There are resonance "mountain ranges" for two values of L_l and there are four peaks which stand out of the mountain ranges. The mountain ranges correspond to a L_r -independent process and will therefore be due to AR. This is confirmed by figure 9b showing in a cut along one of the mountain ranges the AR and the CAR component separately. Figure 9b also

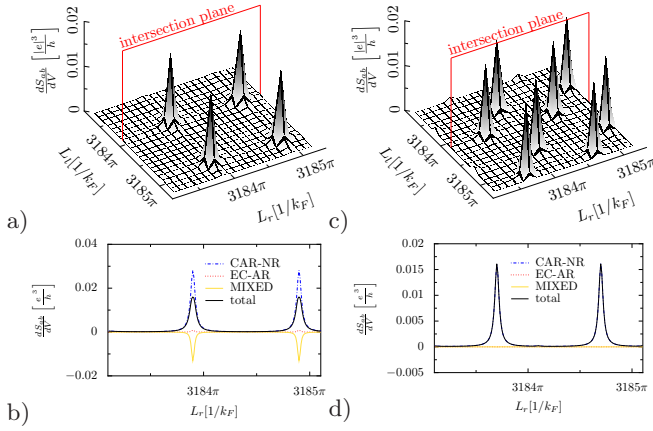


Figure 11: Differential current cross-correlations for $V_a = V_b$ in the tunneling limit $T_{lns} = T_{rsn} = 0.01$, $T_{lnn} = T_{rnn} = 0.26$, a) as a function of L_r and L_l at low voltage $|e|V = 1 \cdot 10^{-4}\Delta$, b) cut through a) at $L_l = 3183.9\pi/k_F$ at higher resolution, c) as a function of L_r and L_l at higher voltage $|e|V = 6.25 \cdot 10^{-2}\Delta$, d) cut through c) at $L_l = 3184.1\pi/k_F$ at higher resolution.

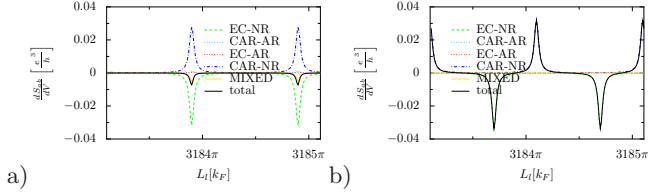


Figure 12: Differential current cross-correlations for $V_a = 0$ in the tunneling limit $T_{lns} = T_{rsn} = 0.01$, $T_{lnn} = T_{rnn} = 0.26$. The three-dimensional plots for the current cross-correlations are quasi-identical to the ones for the nonlocal conductance in figure 10, therefore only the cuts are shown. a) $L_r = 3183.9\pi/k_F$, $|e|V = 1 \cdot 10^{-4}\Delta$, b) $L_r = 3183.6\pi/k_F$, $|e|V_b = 6.25 \cdot 10^{-2}\Delta$

shows that the mountain peaks are due to CAR. The relative distance of two subsequent resonance peaks in units of k_F is π in L_r and in L_l direction. But the absolute resonance positions are not given by integer multiples of π as it would be the case in a simple optical Fabry-Perot interferometer with two identical mirrors. Figure 9c shows the differential conductance at higher voltage (but still much smaller than the gap). As expected from section VA, the AR mountain ranges disappear because the electron and hole resonances do not overlap anymore. Every CAR peak splits up into two peaks corresponding to the two CAR contributions.

The observation of the disappearance of AR and the splitting of the CAR peaks is already interesting in itself. As the peaks are uniquely due to CAR processes, the desired filtering of the different processes contributing to the conductance is achieved. A NNSNN-system operated with symmetrical bias at energies where AR is suppressed and tuned to a CAR resonance peak could be a good source of entangled electrons.

2. Non-local conductance for $V_a = 0$, $V_b > 0$

Figure 10 depicts the calculated differential nonlocal conductance for the biases $V_a = 0$, $V_b > 0$. Panel a) shows the nonlocal differential conductance $dI_a/dV_b|_{V_a=0}$ as a function of the distances L_l and L_r at very low voltage V_b . There are two resonance peaks on the diagonal, where $L_l = L_r$, and two additional resonance peaks where $L_l = L_r \pm \pi/k_F$. From the considerations in the last section, we expect the EC and the CAR resonances to appear at the same positions. As the peaks are negative, the EC contribution is apparently stronger than the CAR contribution. Figure 10b showing a cut through figure 10a at constant L_l , where the total current is decomposed into its EC and CAR component, confirms that the peaks in the three-dimensional plot are indeed a superposition of EC and CAR.

When V_b is increased, the EC and the CAR resonance move apart (see figure 10c). As expected, the EC peaks stay on the diagonals and at $L_l = L_r \pm \pi/k_F$, but their positions are shifted to lower length values. The positive conductance peaks due to CAR appear at the same L_r value as the EC resonance peaks, as both processes are carried by holes on the right hand side. On the left hand side CAR is carried by electrons whose wave vector q^+ decreases with increasing voltage V_b . Consequently, the L_l values of the peak position increase with increasing voltage. Again, the desired filtering of different processes is obtained. This voltage configuration is interesting as the conductance switches between positive and negative values if L_r is changed.

3. Differential current cross-correlations

The differential current cross-correlations $dS_{ab}/dV|_{V_a=V_b=V}$ depicted in figure 11 and $dS_{ab}/dV_b|_{V_a=0}$ depicted in figure 12 behave very similarly to the corresponding differential conductance if one compares the CAR-NR component of the current cross-correlations with the CAR component of the conductance and the EC-NR component with the EC component. The only striking difference is the absence of the "mountain range" in the noise at low symmetrical bias. The similarity between current cross-correlations and conductance has already been discussed at the end of section III in connection to the work of Bignon *et al.*¹¹: As the barriers are opaque, the most likely process to occur is normal reflection. Therefore, the elements of the scattering matrix corresponding to normal reflection are close to one and EC-NR is similar to EC and CAR-NR is similar to CAR. Only the AR component of the conductance has no counterpart in the current cross-correlations, because all elements of the current cross-correlations are composed of a local and a nonlocal process. An AR-NR component does not exist and the AR mountain range is absent in the noise.

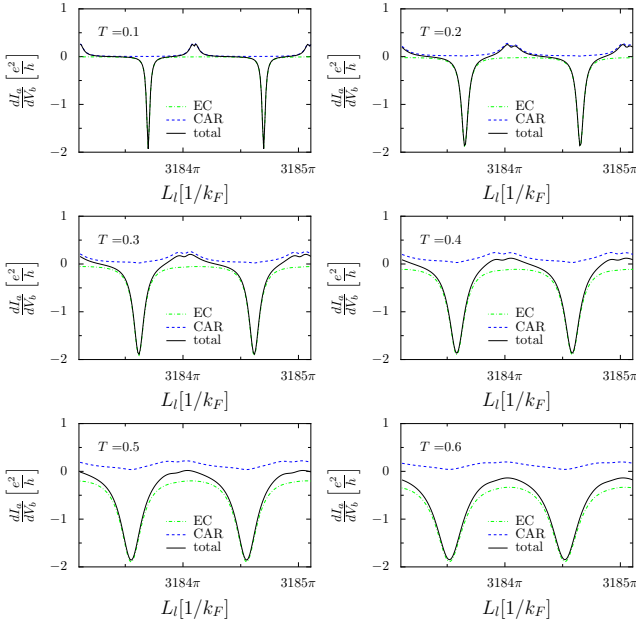


Figure 13: Non-local conductance at $|e|V_b = 6.25 \cdot 10^{-2} \Delta$ and $V_a = 0$ for $T_{l_{nn}} = T_{l_{ns}} = T_{r_{sn}} = T_{r_{nn}} = T$ as indicated in the figure, for a very short superconducting electrode $R = 0.25\xi$, at constant L_r value, chosen to be in resonance so that the conductance in function of L_l features CAR and EC peaks. The CAR peak splits up in two peaks. For $T = 0.5$ and larger, the CAR peak has completely disappeared.

C. Increasing the Interface Transparency

In the last section, we have studied the ballistic system in the tunnel regime where all resonance peaks are sharp. However, the systems in which electronic Fabry-Perot interferences have already been observed, for example^{30,31}, were in the opposite regime of high interface transparency. For increased barrier transparencies, one expects the resonance peaks to become broader and the separation of the different peaks to become less pronounced. This section discusses whether it is necessary to stay in the tunnel regime or if the filtering effect survives to higher interface transparencies.

To investigate systematically what happens when the interface transparency is increased, the nonlocal conductance at $eV_b = 6.25 \cdot 10^{-2} \Delta$ and $V_a = 0$ was calculated for different barrier transparencies, at constant L_r value, which was chosen to be in resonance so that the conductance in function of L_l would feature CAR and EC peaks. Figure 13 shows this conductance for a short superconducting electrode $R = 0.25\xi$ and for different values of $T_{l_{nn}} = T_{l_{ns}} = T_{r_{sn}} = T_{r_{nn}} = T$. The CAR peak shows an interesting feature: It splits up into two peaks, while the EC peak does not. One possible explanation is the interplay between the resonance in the NNS double barrier and the resonance in the central superconductor, both involving Andreev reflections. The first one implies De Gennes-Saint-James bound states³²,

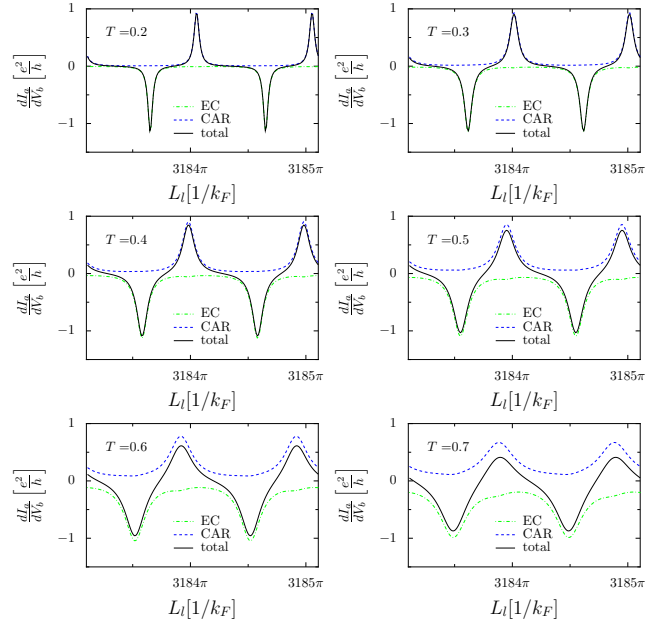


Figure 14: Non-local conductance at $eV_b = 6.25 \cdot 10^{-2} \Delta$ and $V_a = 0$ for $T_{l_{nn}} = T_{l_{ns}} = T_{r_{sn}} = T_{r_{nn}} = T$ as indicated in the figure, for a slightly longer superconducting electrode $R = \xi$, at constant L_r value, chosen to be in resonance so that the conductance in function of L_l features CAR and EC peaks. The EC and CAR peaks are sharper than in the case of the extremely short superconducting electrode depicted in figure 13 and there is no splitting. Even for barrier transparencies as high as $T = 0.7$ the signature of the EC and the CAR contribution is clearly visible.

broadened by the presence of infinite reservoirs. The second are the Tomasch-Rowell-McMillan³³ resonances, due to a scattering between quasiparticle states with different wavevectors k^+, k^- in S. In a NS bilayer, these two processes can altogether lead to a doubling of the resonance peaks³⁴. In the present case, such a doubling is observed in the CAR channel, but is absent in the EC channel where all wavevectors are approximately equal. Moreover, higher transmissions favour the EC channel, and the CAR peak gets weakened altogether.

The amplitude of the quasiparticle wavefunction decreases exponentially with the superconducting length. Therefore, one can hope to decrease the coupling between the two resonances by elongating the superconducting electrode. This actually works, as the plots in figure 14 where $R = \xi$ show: The EC and CAR peaks are sharper than in the case of the extremely short superconducting electrode and there is no splitting. Even for barrier transparencies as high as $T = 0.7$, the signature of the EC and the CAR contribution is clearly visible. Against the general trend, we have here a situation where a longer distance in the superconductor leads to a larger signal.

In conclusion, it is not necessary to operate the NNSN device in the tunnel regime in order to filter the different processes. Surprisingly, CAR resonances are better resolved if the distance in the superconducting

electrode is not too short.

Let us now study a system for intermediate interface transparencies $T = T_{l_{nn}} = T_{l_{ns}} = T_{r_{sn}} = T_{r_{nn}} = 0.5$ and $R = \xi$, which is clearly outside the tunnel regime but has still a good resolution between the different processes, in more detail. We proceed in the same way as in the tunnel regime and analyze the conductance and the current cross-correlations in two different voltage configurations.

1. Conductance for a symmetrically biased system

Figure 15 shows the differential conductance for a symmetrically biased system. At low energies (figure 15a) the predominant structures are again the AR "mountain ranges". But in contrast to the situation in the tunnel regime, there are no CAR peaks on top of the mountain ranges. Instead, at the positions we would have expected them, there are depressions. The cut along the mountain range (figure 15b) shows that the AR component features a deep depression where $L_r = L_l$. This depression already exists in the tunnel regime (figure 9b), but is much less pronounced there. The CAR component increases when L_r approaches L_l as if a peak was to form, but falls back to zero at $L_r = L_l$. We can understand these dips in the conductance from the competition of the different processes at the level of the scattering matrix. At $L_r = L_l = 3183.7\pi/k_F$, EC processes are in resonance (see section VC 2). As the probabilities for the four possible processes have to sum up to one, a large EC scattering matrix element is only possible at the cost of the CAR and AR scattering matrix elements. In the tunnel regime, the most probable process is normal reflection. The EC scattering matrix element can be increased at the cost of the NR scattering matrix element which has no signature in the conductance. But here, the AR contribution is as high as $3.3e^2/h$, while the maximal possible value in a four channel system is $4e^2/h$.

If higher voltages are applied (see figure 15c), each mountain range splits up into two less high mountain ranges. In the tunnel regime, the AR contribution disappears at higher voltage. Electrons and holes have different wavevectors and therefore different resonance lengths and if the resonances are narrow, electrons and holes are not in resonance at the same time. Here with the higher interface transparencies, the resonances are wider and if the electron is in resonance the hole part is still large enough to form a peak and vice versa. At higher applied voltage, the mountain ranges are surmounted by CAR peaks. The resonance of the EC elements of the scattering matrix occur at different values of L_r and CAR and EC are not in direct competition. The AR contribution (figure 15 d) features at higher voltage two depressions, where there was only one at lower voltage. In one case AR is decreased in favor of CAR and in the second case, on the diagonals where $L_r = L_l \text{ mod } \pi/k_F$, it is decreased, as in the low energy case, in favor of EC.

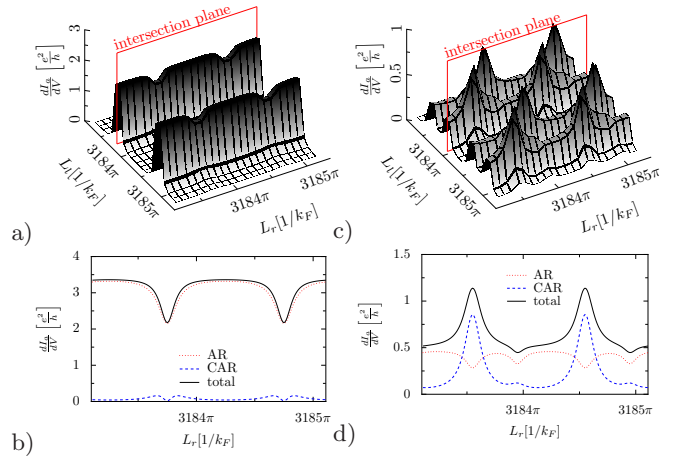


Figure 15: Differential conductance for symmetrically applied bias $V = V_a = V_b$ for intermediate interface transparency $T = T_{l_{nn}} = T_{l_{ns}} = T_{r_{sn}} = T_{r_{nn}} = 0.5$ and $R = \xi$, a) as a function of L_r and L_l at low voltage $|e|V = 1 \cdot 10^{-4}\Delta$, b) cut through a) along one of the mountain ranges (at $L_l = 3183.7\pi/k_F$) at higher resolution, c) as a function of L_r and L_l at higher voltage $|e|V = 6.25 \cdot 10^{-2}\Delta$, d) cut through c) at $L_l = 3183.9\pi/k_F$ at higher resolution.

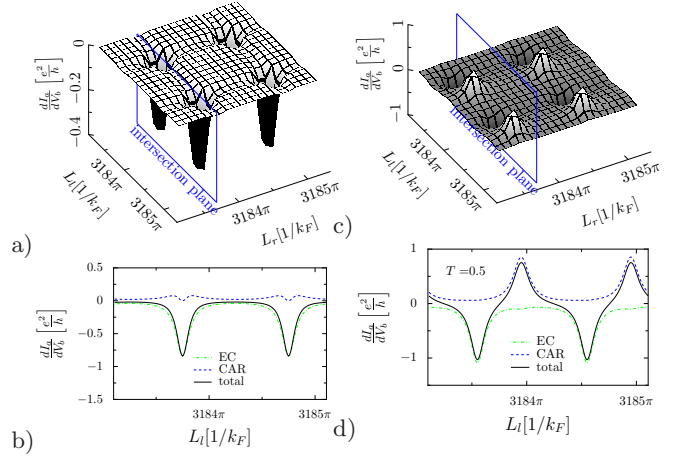


Figure 16: Differential nonlocal conductance $V_a = 0$ for intermediate interface transparency $T = T_{l_{nn}} = T_{l_{ns}} = T_{r_{sn}} = T_{r_{nn}} = 0.5$ and $R = \xi$, a) as a function of L_r and L_l at low voltage $|e|V_b = 1 \cdot 10^{-4}\Delta$, b) cut through a) at $L_r = 3183.7\pi/k_F$ at higher resolution, c) as a function of L_r and L_l at higher voltage $|e|V_b = 6.25 \cdot 10^{-2}\Delta$, d) cut through c) at $L_r = 3183.9\pi/k_F$ at higher resolution.

2. Nonlocal conductance for $V_a = 0, V_b > 0$

Figure 16 shows the nonlocal conductance. The peak positions at both studied voltages have the same symmetry as for the nonlocal conductance in the tunnel regime. But the peaks and depressions are less sharp and are higher. In the tunnel regime, the EC and the CAR peak being superimposed at low voltage were similar in magnitude. On figure 16b however, the EC amplitude is much larger than the CAR amplitude. As in the symmetrically

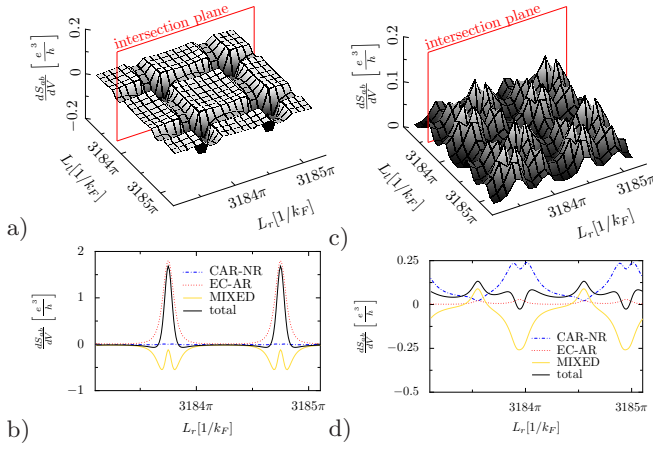


Figure 17: Differential current cross-correlations for symmetrically applied bias $V = V_a = V_b$ for intermediate interface transparency $T = T_{l_{nn}} = T_{l_{ns}} = T_{r_{sn}} = T_{r_{nn}} = 0.5$ and $R = \xi$,
a) as a function of L_r and L_l at low voltage $|e|V = 1 \cdot 10^{-4} \Delta$,
b) cut through a) along one of the mountain ranges (at $L_l = 3183.7\pi/k_F$) at higher resolution,
c) as a function of L_r and L_l at higher voltage $|e|V = 6.25 \cdot 10^{-2} \Delta$,
d) cut through c) at $L_l = 3183.5\pi/k_F$ at higher resolution,

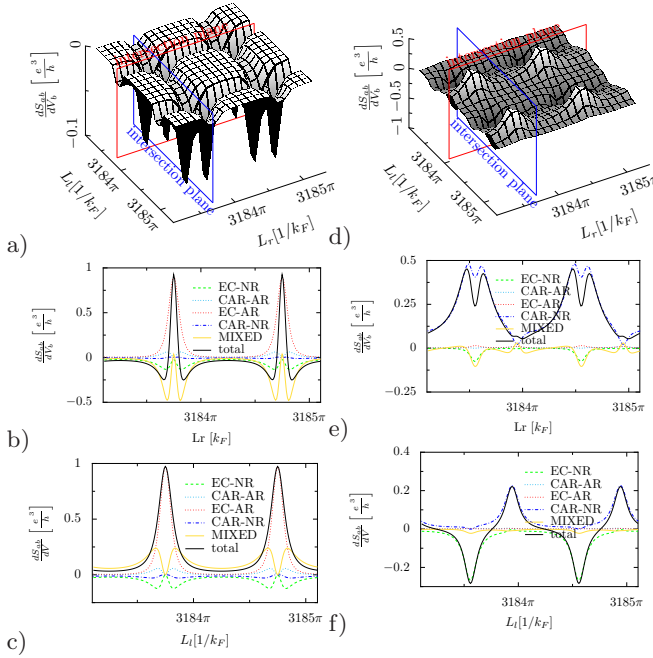


Figure 18: Differential current cross-correlations for $V_a = 0$ for intermediate interface transparency $T = T_{l_{nn}} = T_{l_{ns}} = T_{r_{sn}} = T_{r_{nn}} = 0.5$ and $R = \xi$,
a) as a function of L_r and L_l at low voltage $|e|V_b = 1 \cdot 10^{-4} \Delta$,
b) cut through a) at $L_l = 3183.7\pi/k_F$ at higher resolution,
c) cut through a) at $L_r = 3183.7\pi/k_F$ at higher resolution,
d) as a function of L_r and L_l at higher voltage $|e|V_b = 6.25 \cdot 10^{-2} \Delta$,
e) cut through d) at $L_l = 3183.5\pi/k_F$ at higher resolution,
f) cut through d) at $L_r = 3183.7\pi/k_F$ at higher resolution.

biased case, there is no CAR peak, but the forming peak features a crater. This figure illustrates that the dip in the CAR contribution occurs exactly at the peak position in the EC contribution, indicating that the competition between CAR and EC at the level of the scattering matrix is at the origin of the crater in the CAR peak.

3. Differential current cross-correlations for a symmetrically applied bias

Figure 17 shows the current cross-correlations for the symmetrical bias case. In the tunnel regime the current cross-correlations were dominated by CAR-NR and EC-NR as those processes depend only quadratically on the interface transparency, while MIXED has a cubic and CAR-AR, EC-AR even a bi-quadratic dependence on the interface transparency. For the current cross-correlations at intermediate interface transparency, this restriction does no longer exist. The current cross-correlations in figure 17a feature trenches in L_r and in L_l direction. Their spatial extension lets us conclude that they are connected to the AR amplitude which is independent of L_r respectively L_l . From figure 17b, we see that the trenches are due to MIXED. Figure 17b shows also that the EC-AR component leads to sharp peaks at the positions where $L_r = L_l \bmod \pi/k_F$. These peaks are too narrow to be resolved in the surface plot 17a. Here we have again an example of positive current cross-correlations which are not due to CAR. The CAR-NR component which was dominant in the tunnel regime is almost zero here, which is consistent with the small amplitude of the CAR process observed in the differential conductance.

At higher energies (figures 17d), the CAR-NR contribution gains importance as the scattering matrix elements for CAR and EC are no longer in resonance at the same position. In contrast to the tunnel regime, and like in the case of lower energies, the MIXED processes play an important role.

4. Differential current cross-correlations for $V_a = 0$, $V_b > 0$

The current cross-correlations in the nonlocal conductance bias configuration shown in figure 18 feature at low energy, like the ones in the symmetrically biased case, trenches where the AR parts of the scattering matrix are in resonance. The MIXED component of the current cross-correlations plays an important role and leads together with the EC-NR component to mainly negative current cross-correlations. At the points where $L_r = L_l \bmod \pi/k_F$ and the EC elements of the scattering matrix are in resonance, the EC-AR component leads to positive peaks. At higher applied voltage, there is again the separation of the L_l values where CAR or EC is in resonance, and MIXED becomes less important.

5. Discussion

The above results show that it is not necessary to be in the tunneling limit in order to separate the different components of the conductance. Against the intuitive trend, the distance in the superconductor should not be too short. Owing to multiple scattering at the different interfaces, this can be understood as an optimum in terms of the CAR transmission, with respect to the normal barrier transmissions. In this case, the width and the height of the resonances in the conductance are wider than in the tunnel regime, which could even facilitate their observation. As far as the current cross-correlations are concerned, they are richer but also more difficult to interpret in the regime of intermediate interface transparencies because more components play a role.

VI. COULD THESE EFFECTS BE OBSERVED EXPERIMENTALLY?

What are the possibilities and obstacles for an experimental observation of the phenomena discussed in this chapter? The Fabry-Perot effect needs ballistic transport in a system with only a few (one) channels. The authors of the pioneering paper Ref. 30 observed Fabry-Perot interferences in single-walled nanotubes. Instead of varying the length of the nanotube, they change the Fermi level position in the nanotube by tuning the voltage applied to a gate under the nanotube. As the resonance position depends on the product of wavenumber and length, changing the Fermi wavelength has the same effect as changing the distance between barriers. This strategy is more realistic than to vary the distances L_l and L_r . However, if the electrons in the nanotube are sensitive to the electrostatic potential of a gate, they cannot be perfectly screened. One would have to find a regime where the Coulomb interaction is small enough to be neglected in comparison to the, at least in the tunnel regime, also very small coupling energy between the nanotube and the reservoir, but high enough that the Fermi wave vector can be influenced by a gate.

One could imagine a device consisting of two normal conducting and a superconducting electrode connected by one long carbon nanotube with a symmetry similar to devices with nanowires used in recent experiments^{21,35-37} where the normal and superconducting electrodes are connected over quantum dots. But while there, the system was operated in the Coulomb blockade regime, we need the other extreme of very small Coulomb energy. On both sides of the superconductor, there has to be a gate that can be separately tuned so that several periods of Fabry-Perot interferences can be swept in order to obtain plots similar to the one presented in the last section.

The next question concerns the interfaces. In Ref. 30, where Fabry-Perot interferences are observed, the nanotube is connected with near-perfect ohmic contacts to

the electrodes. This implies a regime of high interface transparencies ($T \approx 1$), not a tunnel regime. If the interface transparency is high, the requirement for the charging energy to be much smaller than the coupling energy is easier to meet, but in the extreme case of $T \approx 1$ the contrast is too small. In the example of Ref.30 the minimal measured conductance is $dI/dV \approx 3.1e^2/h$ and the maximal measured one $dI/dV \approx 3.3e^2/h$. The last section showed that it is not necessary to be in the tunnel regime to obtain a separation of the different contributions to the conductance. This can give hope that an intermediate value of interface transparency can be found. The next problem will then be to achieve this interface transparency experimentally. In addition, for sharp Fabry-Perot interferences, the length of the nanotube has to be well defined. If one uses only one long nanotube the superconducting region is created by the proximity effect in the nanotube. So one cannot really speak of a sharp interface.

In conclusion, it will be challenging to construct a device where the separation of the different components of the conductance and of the current cross-correlations by interference effects in absence of electron-electron interaction are observable. It could nevertheless be possible to reach an experimental regime where Fabry-Perot interference effects are in competition with Coulomb blockade effects. The present analysis of a simplified model describing an extreme case could help to explain such experiments in an intermediate regime and it is a good basis for a more complete theory.

VII. CONCLUSION

We have shown that positive current cross-correlations in the tunnel regime cannot be enhanced with additional barriers by a process similar to reflectionless tunneling, if an average (here, over the interbarrier lengths) has to be performed, mimicking disorder landscapes which are uncorrelated on the two sides of the set-up. In analogy, one cannot therefore expect that the use of diffusive normal metals will facilitate the experimental observation of positive current cross-correlations. This negative conclusion is important for experiments.

On the contrary, the insertion of additional tunnel barriers into ballistic NSN-devices leads to Fabry-Perot like oscillations of the differential conductance and of the current cross-correlations. The resonances for different processes are well separated at finite energy, because of the different energy dependence of electron and hole wave vectors and CAR and EC processes can be efficiently filtered for intermediate transparencies and for a central superconductor width of the order of the coherence length.

Acknowledgements

The authors have benefited from several fruitful discussions with B. Douçot. Part of this work was supported by ANR Project "Elec-EPR".

Appendix A: Details on the scattering approach

The elements $s_{ij}^{\alpha\beta}$ of the scattering matrix are calculated within the BTK approach²⁶: Two-component wavefunctions, where the upper component describes electrons and the lower components holes, are matched at the interfaces and the coefficients of the resulting system of equations give the elements of the scattering matrix. In the normal conductors the the wavefunctions are plane waves with wavevectors close to the Fermi wavevector $\hbar k_F = \sqrt{2m\mu}$. The wavevector for electrons reads $\hbar q^+ = \sqrt{2m\sqrt{\mu + E}}$, the one for holes $\hbar q^- = \sqrt{2m\sqrt{\mu - E}}$. In the superconductor, the wavefunction has to obey the Bogoliubov-De Gennes equation, where the supercon-

ducting gap is supposed to be a positive constant inside the superconductor and zero outside of it. This is achieved by modifying the amplitudes of the wavefunction in the superconductor with the coherence factors u_E and v_E which read for energies smaller than the gap ($E < \Delta$):

$$u_E = \frac{1}{\sqrt{2}} \sqrt{1 + \frac{i\sqrt{\Delta^2 - E^2}}{E}}, \quad v_E = \frac{1}{\sqrt{2}} \sqrt{1 - \frac{i\sqrt{\Delta^2 - E^2}}{E}} \quad (\text{A1})$$

and by using for quasi-particles proportional to $\begin{pmatrix} u_E \\ v_E \end{pmatrix}$ the wavevector $\hbar k^+ = \sqrt{2m}\sqrt{\mu + i\sqrt{\Delta^2 - E^2}}$ and for quasi-particles proportional to $\begin{pmatrix} v_E \\ u_E \end{pmatrix}$ the wavevector $\hbar k^- = \sqrt{2m}\sqrt{\mu - i\sqrt{\Delta^2 - E^2}}$. For example, the wavefunctions for an electron incoming from electrode N_a take the form

$$\psi_{N_a}(x) = \begin{pmatrix} 1 \\ 0 \end{pmatrix} \left(1 e^{iq^+x} + s_{aa}^{ee} e^{-iq^+x} \right) + \begin{pmatrix} 0 \\ 1 \end{pmatrix} \left(s_{aa}^{he} e^{iq^-x} + 0 e^{-iq^-x} \right), \quad (\text{A2})$$

$$\psi_{N_l}(x) = \begin{pmatrix} 1 \\ 0 \end{pmatrix} \left(c_1 e^{iq^+x} + c_2 e^{-iq^+(x-L_l)} \right) + \begin{pmatrix} 0 \\ 1 \end{pmatrix} \left(c_3 e^{iq^-x} + c_4 e^{-iq^-(x-L_l)} \right), \quad (\text{A3})$$

$$\begin{aligned} \psi_S(x) &= \begin{pmatrix} u_E \\ v_E \end{pmatrix} \left(c_5 e^{ik^+(x-L_l)} + c_6 e^{-ik^+(x-L_l-R)} \right) \\ &+ \begin{pmatrix} v_E \\ u_E \end{pmatrix} \left(c_7 e^{-ik^-(x-L_l)} + c_8 e^{ik^-(x-L_l-R)} \right), \end{aligned} \quad (\text{A4})$$

$$\begin{aligned} \psi_{N_r}(x) &= \begin{pmatrix} 1 \\ 0 \end{pmatrix} \left(c_9 e^{iq^+(x-L_l-R)} + c_{10} e^{-iq^+(x-L_l-R-L_r)} \right) \\ &+ \begin{pmatrix} 0 \\ 1 \end{pmatrix} \left(c_{11} e^{iq^-(x-L_l-R)} + c_{12} e^{-iq^-(x-L_l-R-L_r)} \right), \end{aligned} \quad (\text{A5})$$

$$\begin{aligned} \psi_{N_b}(x) &= \begin{pmatrix} 1 \\ 0 \end{pmatrix} \left(s_{b,a}^{e,e} e^{iq^+(x-L_l-R-L_r)} + 0 e^{-iq^+(x-L_l-R-L_r)} \right) \\ &+ \begin{pmatrix} 0 \\ 1 \end{pmatrix} \left(0 e^{iq^-(x-L_l-R)} + s_{b,a}^{h,e} e^{-iq^-(x-L_l-R-L_r)} \right) \end{aligned} \quad (\text{A6})$$

in the sections N_a , N_l , S , N_r , and N_b respectively [see Fig. 1] and give access to the scattering matrix elements $s_{a,a}^{e,e}$, $s_{a,a}^{h,e}$, $s_{b,a}^{h,e}$ and $s_{b,a}^{e,e}$. The remaining elements of the scattering matrix can be obtained from the other possible scattering processes i.e. a hole incoming from electrode N_a , an electron/hole incoming from electrode N_b .

The interfaces are modeled by δ -potentials $V(x) = Z\hbar v_F \delta(x)$, where the BTK parameter Z is connected to the interface transparency T by $T = (1 + Z^2)^{-1}$. The elements of the scattering matrix can be determined and the constants c_i eliminated using

the continuity of the wavefunctions at the interfaces [$\psi_{N_a}(0) = \psi_{N_l}(0)$ etc.] and the boundary condition for the derivatives [$\psi'_{N_l}(0) - \psi'_{N_a}(0) = Z\hbar v_F \psi_a(0)$ etc.] at every interface.

In simple cases, i. e. for only two or three sections and in the limit of zero energy, the system of equations giving the scattering matrix elements can be solved analytically (see¹⁸), but in the present case of five section the expressions become so unhandy that we decided to solve the the equations numerically.

Appendix B: Components of Current Cross Correlations

Components of the current cross-correlations:

$$\begin{aligned}
s_{ab}(T=0, V_a, V_b) = \frac{2e^2}{h} \int dE \left(\right. \\
& 2\Re \left[s_{ab}^{ee} s_{ba}^{ee} s_{aa}^{ee\dagger} s_{bb}^{ee\dagger} \right] (\theta(|e|V_a - E) - 2\theta(|e|V_a - E)\theta(|e|V_b - E) + \theta(|e|V_b - E)) \\
& + 2\Re \left[s_{ab}^{hh} s_{ba}^{hh} s_{aa}^{hh\dagger} s_{bb}^{hh\dagger} \right] (\theta(-|e|V_a - E) - 2\theta(-|e|V_a - E)\theta(-|e|V_b - E) + \theta(-|e|V_b - E)) \left. \right\} EC - NR \\
& + 2\Re \left[s_{ba}^{eh} s_{ab}^{he} s_{aa}^{hh\dagger} s_{bb}^{ee\dagger} \right] (-\theta(-|e|V_a - E) + 2\theta(-|e|V_a - E)\theta(|e|V_b - E) - \theta(|e|V_b - E)) \\
& + 2\Re \left[s_{ab}^{eh} s_{ba}^{he} s_{aa}^{ee\dagger} s_{bb}^{hh\dagger} \right] (-\theta(|e|V_a - E) + 2\theta(|e|V_a - E)\theta(-|e|V_b - E) - \theta(-|e|V_b - E)) \left. \right\} CAR - NR \\
& + 2\Re \left[s_{ab}^{hh} s_{ba}^{ee} s_{bb}^{eh\dagger} s_{aa}^{he\dagger} \right] (-\theta(|e|V_a - E) + 2\theta(|e|V_a - E)\theta(-|e|V_b - E) - \theta(-|e|V_b - E)) \\
& + 2\Re \left[s_{ab}^{ee} s_{ba}^{hh} s_{aa}^{eh\dagger} s_{bb}^{he\dagger} \right] (-\theta(-|e|V_a - E) + 2\theta(-|e|V_a - E)\theta(|e|V_b - E) - \theta(|e|V_b - E)) \left. \right\} EC - AR \\
& + 2\Re \left[s_{ba}^{he} s_{ab}^{eh} s_{aa}^{he\dagger} s_{bb}^{he\dagger} \right] (\theta(|e|V_a - E) - 2\theta(|e|V_a - E)\theta(|e|V_b - E) + \theta(|e|V_b - E)) \\
& + 2\Re \left[s_{ab}^{eh} s_{ba}^{he} s_{aa}^{eh\dagger} s_{bb}^{he\dagger} \right] (\theta(-|e|V_a - E) - 2\theta(-|e|V_a - E)\theta(-|e|V_b - E) + \theta(-|e|V_b - E)) \left. \right\} CAR - AR \\
& + 2\Re \left[s_{ab}^{eh} s_{ba}^{hh} s_{bb}^{hh\dagger} s_{aa}^{eh\dagger} + s_{ab}^{hh} s_{ba}^{eh} s_{aa}^{hh\dagger} s_{bb}^{eh\dagger} \right] (-\theta(-|e|V_a - E) + 2\theta(-|e|V_a - E)\theta(-|e|V_b - E) - \theta(-|e|V_b - E)) \\
& + 2\Re \left[s_{ab}^{ee} s_{ba}^{he} s_{aa}^{ee\dagger} s_{bb}^{he\dagger} + s_{ab}^{he} s_{ba}^{ee} s_{aa}^{ee\dagger} s_{bb}^{he\dagger} \right] (-\theta(|e|V_a - E) + 2\theta(|e|V_a - E)\theta(|e|V_b - E) - \theta(|e|V_b - E)) \left. \right\} MIXED1 \\
& + 2\Re \left[s_{ab}^{ee} s_{ba}^{eh} s_{bb}^{eh\dagger} s_{aa}^{he\dagger} + s_{ab}^{eh} s_{ba}^{ee} s_{aa}^{eh\dagger} s_{bb}^{he\dagger} \right] (\theta(-|e|V_a - E) - 2\theta(-|e|V_a - E)\theta(|e|V_b - E) + \theta(|e|V_b - E)) \\
& + 2\Re \left[s_{ab}^{eh} s_{ba}^{ee} s_{aa}^{ee\dagger} s_{bb}^{eh\dagger} + s_{ab}^{ee} s_{ba}^{eh} s_{aa}^{ee\dagger} s_{bb}^{eh\dagger} \right] (\theta(-|e|V_a - E) - 2\theta(-|e|V_a - E)\theta(|e|V_b - E) + \theta(|e|V_b - E)) \left. \right\} MIXED2 \\
& + 2\Re \left[s_{aa}^{hh} s_{ba}^{ee} s_{bb}^{eh\dagger} s_{aa}^{he\dagger} + s_{aa}^{ee} s_{ba}^{hh} s_{bb}^{eh\dagger} s_{aa}^{he\dagger} \right] (-\theta(|e|V_a - E) + 2\theta(|e|V_a - E)\theta(-|e|V_a - E) - \theta(-|e|V_a - E)) \\
& + 2\Re \left[s_{ab}^{hh} s_{bb}^{ee} s_{bb}^{eh\dagger} s_{bb}^{he\dagger} + s_{ab}^{ee} s_{bb}^{hh} s_{bb}^{eh\dagger} s_{bb}^{he\dagger} \right] (-\theta(|e|V_b - E) + 2\theta(|e|V_b - E)\theta(-|e|V_b - E) - \theta(-|e|V_b - E)) \\
& + 2\Re \left[s_{aa}^{eh} s_{ba}^{ee} s_{aa}^{eh\dagger} s_{ba}^{he\dagger} + s_{ba}^{he} s_{aa}^{ee} s_{aa}^{eh\dagger} s_{ba}^{he\dagger} \right] (\theta(|e|V_a - E) - 2\theta(|e|V_a - E)\theta(-|e|V_a - E) + \theta(-|e|V_a - E)) \\
& + 2\Re \left[s_{ab}^{ee} s_{ab}^{eh} s_{bb}^{eh\dagger} s_{ab}^{he\dagger} + s_{ab}^{eh} s_{ab}^{ee} s_{bb}^{eh\dagger} s_{ab}^{he\dagger} \right] (\theta(|e|V_b - E) - 2\theta(|e|V_b - E)\theta(-|e|V_b - E) + \theta(-|e|V_b - E)) \left. \right\} MIXED4b
\end{aligned}$$

Differential current cross-correlations in the nonlocal conductance setup:

$$\begin{aligned}
\frac{dS_{ab}(T=0, V_a=0, V_b)}{dV_b} = \frac{2|e|^3}{h} \text{sgn}(V_b) \left(\right. \\
& 2\Re \left[s_{ab}^{ee} (|e|V_b) s_{ba}^{ee} (|e|V_b) s_{aa}^{ee\dagger} (|e|V_b) s_{bb}^{ee\dagger} (|e|V_b) \right] + 2\Re \left[s_{ab}^{hh} (-|e|V_b) s_{ba}^{hh} (-|e|V_b) s_{aa}^{hh\dagger} (-|e|V_b) s_{bb}^{hh\dagger} (-|e|V_b) \right] \left. \right\} EC - NR \\
& - 2\Re \left[s_{ba}^{eh} (|e|V_b) s_{ab}^{he} (|e|V_b) s_{aa}^{hh\dagger} (|e|V_b) s_{bb}^{ee\dagger} (|e|V_b) \right] - 2\Re \left[s_{ab}^{eh} (-|e|V_b) s_{ba}^{he} (-|e|V_b) s_{aa}^{hh\dagger} (-|e|V_b) s_{bb}^{ee\dagger} (-|e|V_b) \right] \left. \right\} CAR - NR \\
& - 2\Re \left[s_{ab}^{ee} (|e|V_b) s_{ba}^{hh} (|e|V_b) s_{aa}^{ee\dagger} (|e|V_b) s_{bb}^{eh\dagger} (|e|V_b) \right] - 2\Re \left[s_{ab}^{eh} (-|e|V_b) s_{ba}^{ee} (-|e|V_b) s_{bb}^{eh\dagger} (-|e|V_b) s_{aa}^{ee\dagger} (-|e|V_b) \right] \left. \right\} EC - AR \\
& + 2\Re \left[s_{ba}^{he} (|e|V_b) s_{ab}^{eh} (|e|V_b) s_{aa}^{he\dagger} (|e|V_b) s_{bb}^{eh\dagger} (|e|V_b) \right] + 2\Re \left[s_{ab}^{eh} (-|e|V_b) s_{ba}^{he} (-|e|V_b) s_{aa}^{he\dagger} (-|e|V_b) s_{bb}^{eh\dagger} (-|e|V_b) \right] \left. \right\} CAR - AR \\
& - 2\Re \left[s_{ab}^{ee} (|e|V_b) s_{ba}^{he} (|e|V_b) s_{aa}^{ee\dagger} (|e|V_b) s_{bb}^{he\dagger} (|e|V_b) \right] + s_{ba}^{ee} (|e|V_b) s_{ab}^{he} (|e|V_b) s_{bb}^{ee\dagger} (|e|V_b) s_{aa}^{he\dagger} (|e|V_b) \\
& - 2\Re \left[s_{ab}^{eh} (-|e|V_b) s_{ba}^{hh} (-|e|V_b) s_{aa}^{hh\dagger} (-|e|V_b) s_{bb}^{eh\dagger} (-|e|V_b) \right] + s_{ba}^{eh} (-|e|V_b) s_{ab}^{hh} (-|e|V_b) s_{bb}^{eh\dagger} (-|e|V_b) s_{aa}^{hh\dagger} (-|e|V_b) \left. \right\} MIXED1 \\
& + 2\Re \left[s_{ab}^{eh} (|e|V_b) s_{ba}^{ee} (|e|V_b) s_{aa}^{ee\dagger} (|e|V_b) s_{bb}^{eh\dagger} (|e|V_b) \right] + s_{ab}^{hh} (|e|V_b) s_{ba}^{he} (|e|V_b) s_{bb}^{hh\dagger} (|e|V_b) s_{aa}^{he\dagger} (|e|V_b) \\
& + 2\Re \left[s_{ab}^{ee} (-|e|V_b) s_{ba}^{eh} (-|e|V_b) s_{aa}^{ee\dagger} (-|e|V_b) s_{bb}^{eh\dagger} (-|e|V_b) \right] + s_{ba}^{ee} (-|e|V_b) s_{ab}^{eh} (-|e|V_b) s_{bb}^{ee\dagger} (-|e|V_b) s_{aa}^{eh\dagger} (-|e|V_b) \left. \right\} MIXED2 \\
& - 2\Re \left[s_{ab}^{eh} (|e|V_b) s_{bb}^{he} (|e|V_b) s_{aa}^{ee\dagger} (|e|V_b) s_{bb}^{hh\dagger} (|e|V_b) \right] + s_{ab}^{hh} (|e|V_b) s_{bb}^{ee} (|e|V_b) s_{aa}^{he\dagger} (|e|V_b) s_{bb}^{eh\dagger} (|e|V_b) \\
& - 2\Re \left[s_{ab}^{eh} (-|e|V_b) s_{bb}^{he} (-|e|V_b) s_{aa}^{ee\dagger} (-|e|V_b) s_{bb}^{hh\dagger} (-|e|V_b) \right] + s_{ab}^{hh} (-|e|V_b) s_{bb}^{ee} (-|e|V_b) s_{aa}^{he\dagger} (-|e|V_b) s_{bb}^{eh\dagger} (-|e|V_b) \left. \right\} MIXED3b \\
& + 2\Re \left[s_{ab}^{ee} (|e|V_b) s_{ab}^{eh} (|e|V_b) s_{bb}^{eh\dagger} (|e|V_b) s_{ab}^{he\dagger} (|e|V_b) \right] + s_{ab}^{eh} (|e|V_b) s_{bb}^{ee} (|e|V_b) s_{bb}^{hh\dagger} (|e|V_b) s_{ab}^{he\dagger} (|e|V_b) \\
& + 2\Re \left[s_{ab}^{ee} (-|e|V_b) s_{ab}^{eh} (-|e|V_b) s_{bb}^{eh\dagger} (-|e|V_b) s_{ab}^{he\dagger} (-|e|V_b) \right] + s_{ab}^{eh} (-|e|V_b) s_{bb}^{ee} (-|e|V_b) s_{bb}^{hh\dagger} (-|e|V_b) s_{ab}^{he\dagger} (-|e|V_b) \left. \right\} MIXED4b
\end{aligned}$$

Differential current cross-correlations in the symmetrical setup:

$$\begin{aligned}
\frac{dS_{ab}(T=0, V_a=V, V_b=V)}{dV} = \frac{2|e|^3}{h} \text{sgn}(|e|V) \left(\right. \\
& - 2\Re \left[s_{ba}^{eh} (|e|V) s_{ab}^{he} (|e|V) s_{aa}^{hh\dagger} (|e|V) s_{bb}^{ee\dagger} (|e|V) \right] + s_{ab}^{eh} (|e|V) s_{ba}^{he} (|e|V) s_{aa}^{ee\dagger} (|e|V) s_{bb}^{hh\dagger} (|e|V) \\
& - 2\Re \left[s_{ba}^{eh} (-|e|V) s_{ab}^{he} (-|e|V) s_{aa}^{hh\dagger} (-|e|V) s_{bb}^{ee\dagger} (-|e|V) \right] + s_{ab}^{eh} (-|e|V) s_{ba}^{he} (-|e|V) s_{aa}^{ee\dagger} (-|e|V) s_{bb}^{hh\dagger} (-|e|V) \left. \right\} CAR - NR \\
& - 2\Re \left[s_{ab}^{hh} (|e|V) s_{ba}^{ee} (|e|V) s_{aa}^{eh\dagger} (|e|V) \right] + s_{ab}^{ee} (|e|V) s_{ba}^{hh} (|e|V) s_{aa}^{eh\dagger} (|e|V) s_{bb}^{ee\dagger} (|e|V) \\
& - 2\Re \left[s_{ab}^{hh} (-|e|V) s_{ba}^{ee} (-|e|V) s_{aa}^{eh\dagger} (-|e|V) \right] + s_{ab}^{ee} (-|e|V) s_{ba}^{hh} (-|e|V) s_{aa}^{eh\dagger} (-|e|V) s_{bb}^{ee\dagger} (-|e|V) \left. \right\} EC - AR \\
& + 2\Re \left[s_{ab}^{ee} (|e|V) s_{ba}^{eh} (|e|V) s_{aa}^{ee\dagger} (|e|V) s_{bb}^{eh\dagger} (|e|V) \right] + s_{ba}^{ee} (|e|V) s_{ab}^{eh} (|e|V) s_{aa}^{ee\dagger} (|e|V) s_{bb}^{eh\dagger} (|e|V) \\
& + 2\Re \left[s_{ab}^{ee} (-|e|V) s_{ba}^{eh} (-|e|V) s_{aa}^{ee\dagger} (-|e|V) s_{bb}^{eh\dagger} (-|e|V) \right] + s_{ba}^{ee} (-|e|V) s_{ab}^{eh} (-|e|V) s_{aa}^{ee\dagger} (-|e|V) s_{bb}^{eh\dagger} (-|e|V) \\
& + 2\Re \left[s_{ab}^{eh} (|e|V) s_{ba}^{ee} (|e|V) s_{aa}^{ee\dagger} (|e|V) s_{bb}^{eh\dagger} (|e|V) \right] + s_{ab}^{hh} (|e|V) s_{ba}^{he} (|e|V) s_{bb}^{hh\dagger} (|e|V) s_{aa}^{he\dagger} (|e|V) \\
& + 2\Re \left[s_{ab}^{eh} (-|e|V) s_{ba}^{ee} (-|e|V) s_{aa}^{ee\dagger} (-|e|V) s_{bb}^{eh\dagger} (-|e|V) \right] + s_{ab}^{hh} (-|e|V) s_{ba}^{he} (-|e|V) s_{bb}^{hh\dagger} (-|e|V) s_{aa}^{he\dagger} (-|e|V) \left. \right\} MIXED2
\end{aligned}$$

- ²³ A. Kastalsky, A. W. Kleinsasser, L. H. Greene, R. Bhat, F. P. Milliken and J. P. Harbison, Phys. Rev. Lett. **67**, 3026 (1991).
- ²⁴ F. W. J. Hekking and Yu. V. Nazarov, Phys. Rev. Lett. **71**, 1625 (1991); *ibid.*, Phys. Rev. B **49**, 6847 (1994).
- ²⁵ J. A. Melsen and Beenakker C. W. J., Physica B **203**, 219 (1994).
- ²⁶ G. E. Blonder, M. Tinkham, and T. M. Klapwijk, Phys. Rev. B **25**, 4515 (1982).
- ²⁷ M. P. Anantram and S. Datta, Phys. Rev. B **53**, 16390 (1996).
- ²⁸ T. Martin and R. Landauer, Phys. Rev. B **45**, 1742 (1992).
- ²⁹ M. Büttiker, Phys. Rev. Lett. **65**, 2901 (1990).
- ³⁰ W. Liang, M. Bockrath, D. Bozovic, J. H. Hafner, M. Tinkham, H. Park, Nature **411**, 665 (2001).
- ³¹ H. I. Jørgensen, K. Grove-Rasmussen, T. Novotný, K. Flensberg, and P. E. Lindelof, Phys. Rev. Lett. **96**, 207003 (2006).
- ³² P. G. de Gennes and D. Saint-James, Phys. Lett. **4**, 151 (1963); D. Saint-James, J. Phys. (Paris) **25**, 899 (1964).
- ³³ W. J. Tomasch, Phys. Rev. Lett. **15**, 672 (1965); *ibid.*, Phys. Rev. Lett. **16**, 16 (1966); W. L. McMillan and P. W. Anderson, Phys. Rev. Lett. **16**, 85 (1966); J. M. Rowell and W. L. McMillan, Phys. Rev. Lett. **16**, 453 (1966).
- ³⁴ O. Entin-Wohlmann and J. Bar-Sagi, Phys. Rev. B **18**, 3174 (1978).
- ³⁵ L. Hofstetter, S. Csonka, J. Nygård, and C. Schönberger, *Cooper pair splitter realized in a two-quantum-dot Y-junction*, Nature **461**, 960 (2009).
- ³⁶ L. G. Herrmann, F. Portier, P. Roche, A. Levy Yeyati, T. Kontos, and C. Strunk, Phys. Rev. Lett. **104**, 026801 (2010).
- ³⁷ L. Hofstetter, S. Csonka, A. Baumgartner, G. Fülöp, S. d'Hollosy, J. Nygård, and C. Schönberger, Phys. Rev. Lett. **107**, 136801 (2011).